Pet. Sci. (2016) 13:225–236
DOI 10.1007/s12182-016-0092-7

ORIGINAL PAPER

Velocity calibration for microseismic event location using surface data

Hai-Yu Jiang[1] · Zu-Bin Chen[1] · Xiao-Xian Zeng[1] · Hao Lv[1] · Xin Liu[1]

Received: 17 July 2015 / Published online: 20 April 2016

Abstract Because surface-based monitoring of hydraulic fracturing is not restricted by borehole geometry or the difficulties in maintaining subsurface equipment, it is becoming an increasingly common part of microseismic monitoring. The ability to determine an accurate velocity model for the monitored area directly affects the accuracy of microseismic event locations. However, velocity model calibration for location with surface instruments is difficult for several reasons: well log measurements are often inaccurate or incomplete, yielding intractable models; origin times of perforation shots are not always accurate; and the non-uniqueness of velocity models obtained by inversion becomes especially problematic when only perforation shots are used. In this paper, we propose a new approach to overcome these limitations. We establish an initial velocity model from well logging data, and then use the root mean square (RMS) error of double-difference arrival times as a proxy measure for the misfit between the well log velocity model and the true velocity structure of the medium. Double-difference RMS errors are reduced by using a very fast simulated annealing for model perturbance, and a sample set of double-difference RMS errors is then selected to determine an empirical threshold. This threshold value is set near the minimum RMS of the selected samples, and an appropriate number of travel times within the threshold range are chosen. The corresponding velocity models are then used to relocate the perforation-shot. We use the velocity model with the smallest relative location errors as the basis for microseismic location. Numerical analysis with exact input velocity models shows that although large differences exist between the calculated and true velocity models, perforation shots can still be located to their actual positions with the proposed technique; the location inaccuracy of the perforation is <2 m. Further tests on field data demonstrate the validity of this technique.

Keywords Velocity calibration · Microseismic monitoring · Double-difference RMS error · Very fast simulated annealing · Perforation-shot relocation

1 Introduction

Hydraulic fracturing of low-permeability reservoirs generates many microseismic events due to pressure increase associated with fluid injection into treatment wells (Warpinski et al. 2005). Fracture development can be characterized by various microseismic monitoring techniques (Liang et al. 2015; Wang et al. 2013). Generally speaking, when the approximate locations of perforation shots can be resolved, we have the confidence to locate nearby microseismic events, and a usable velocity model plays an important role to achieve this goal (Usher et al. 2013). At present, because of the convenience of operation, surface observations are an effective technique when monitoring wells cannot be used. They are one of the main targets for improvement in future microseismic monitoring. Microseismic monitoring with surface observations

✉ Zu-Bin Chen
czb@jlu.edu.cn

Hai-Yu Jiang
joyjiang1987@126.com

[1] Key Laboratory of Geo-Exploration and Instrumentation of Ministry of Education, College of Instrumentation and Electrical Engineering, Jilin University, Changchun 130026, Jilin, China

Edited by Jie Hao

requires a well-resolved velocity model, yet many factors can interfere with model calibration, as follows. (1) Well logs are influenced by many extraneous factors, such as pore pressure, stress accumulation, and mud invasion; in addition, seismic wave velocities around the reservoir can be altered by prior resource extraction, including mining. Consequently, velocity measurements from well logs are often unsuitable for microseismic event location (Grechka et al. 2011; Pei et al. 2009; Quirein et al. 2006; Zhang et al. 2013a, b). Moreover, log data may be incomplete, which naturally reduces the accuracy of the initial model. Methods based on searching for a local optimal solution (Pei et al. 2008; Tan et al. 2013) are not suitable for this task. (2) A particularly common problem in microseismic monitoring is a combination of little available source information (e.g., perforation shots), few receivers, and poor network coverage, resulting in a poorly constrained velocity model. (3) Perforations are often not precisely timed, so a velocity model cannot always be calibrated using perforation travel times alone. Although seismic tomography is widely used to image earth structure on local to global scales, the above limitations mean that we cannot expect the same high-quality results from microseismic monitoring data (Bardainne and Gaucher 2010). Several papers have proposed methods to construct reservoir velocity models for microseismic event location, most of which are based on the following steps: (1) A simple velocity model, using only a few parameters, is constructed from well logging data. (2) Known positions of perforation shots are iteratively relocated until a suitable velocity model is obtained. Pei et al. (2009) and Bardainne and Gaucher (2010) developed a fast simulated annealing algorithm to invert for a velocity model, which showed little dependence on initial values and outperformed the local optimal solution technique. However, the method still faced the problem that perforation shot origin times are generally inaccurate. Tan et al. (2013) proposed an inversion method based on time differences calculated from picked arrival times, which circumvented the issue of origin time inaccuracies. However, their method was still sensitive to the initial model. Anikiev et al. (2014) described a method in which the initial velocity of each layer was simultaneously increased or decreased using the accuracy of perforation shot relocations as an evaluation standard. They obtained a relatively accurate velocity model by inversion. However, their method still could not satisfy the precision requirements of microseismic event location.

This paper presents a new method to address the problem of velocity model calibration using surface data. A one-dimensional layered model is built, in which the difference between theoretical and expected models is characterized by the root mean square (RMS) errors of time double differences (DDrms) (Concha et al. 2010; Waldhauser and Ellsworth 2000; Zhang et al. 2009a, b; Zhang and Thurber 2003; Zhou et al. 2010). Using the relative differences of the first arrival times of multiple events, DDrms values are minimized using very fast simulated annealing (VFSA) (Pei et al. 2009). In order to obtain an optimal velocity model for perforation relocations, we select a subset of DDrms from the results of simulated annealing. A threshold is set near the minimum value, and velocity models with DDrms values between the threshold and the minimum are chosen for further analysis. These models are then used to relocate the perforation shots. We choose the velocity model with the smallest perforation shot location errors as the model for locating microseismic events.

This paper first introduces the principles of the method, and then conducts tests on synthetic data. We investigate the influences of velocity range constraints and picking errors on the proposed technique. Finally, the proposed technique is applied to data from a perforation shot at a gas shale reservoir as an example of velocity model calculation.

2 Travel time calculation

This study uses ray tracing to obtain travel times for microseismic events and perforation shots. Traditional two-point ray tracing algorithms mainly comprise shooting (e.g., Xu et al. 2004) and ray bending algorithms (e.g., Li et al. 2013). More recent works use wave front extension methods based on the eikonal equation and Huygens' principle (e.g., Zhang et al. 2006a, b); the shortest path algorithm (Wang and Chang 2002; Zhang et al. 2006a, b; Zhao and Zhang 2014); and the LTI method (Zhang et al. 2009a, b), based on graph theory and Fermat's principle. Compared with the above methods, ray tracing based on Snell's law is not restricted by nodes and can provide accurate travel time and azimuth information (Zhang et al. 2013a, b). Traditional shooting methods were improved by Gao and Xu (1996), who proposed a new type of step-by-step iterative ray tracing algorithm that greatly improved computational efficiency. This method can also be used with a slightly more complicated velocity model than other techniques. In this paper, we expand the method to a 3D layered structure for calculating travel times.

2.1 Ray tracing in a layered medium

As shown in Fig. 1, the dichotomy is used to determine the shortest path between two points in difference medium. We set the medium interface to $Z = z_2$, where P_1 is the launch point, P_3 is the receiver, P_2 is the intersection of P_1 and P_3

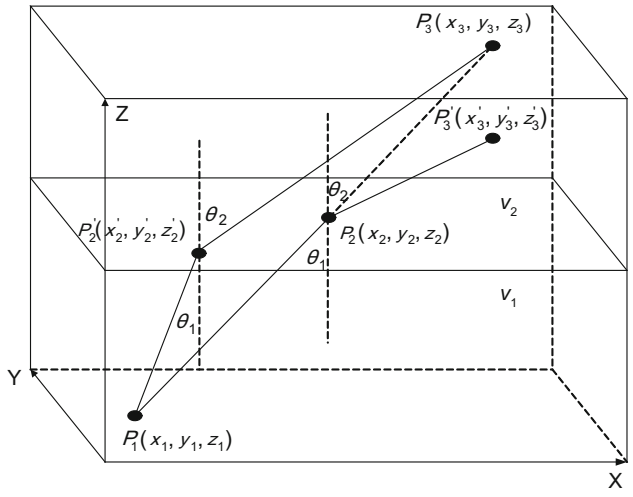

Fig. 1 Solving the refraction points by dichotomy

with the medium interface, and P_3' is the end point of the test ray path.

Beginning with Snell's law of refraction,

$$\frac{\sin\theta_1}{\sin\theta_2}=\frac{v_1}{v_2} \tag{1}$$

and substituting P_1, P_2, P_3' into the equation above, we have

$$\frac{v_1\sqrt{(x_3'-x_2)^2+(y_3'-y_2)^2}}{\sqrt{(x_3'-x_2)^2+(y_3'-y_2)^2+(z_3'-z_2)^2}}=\frac{v_2\sqrt{(x_1-x_2)^2+(y_1-y_2)^2}}{\sqrt{(x_1-x_2)^2+(y_1-y_2)^2+(z_1-z_2)^2}} \tag{2}$$

If $x_3'=x_3$, $y_3'=y_3$, then

$$a=\frac{c(1-b^2)}{b^2} \tag{3}$$

$$\begin{cases} z_3'=z_3+\sqrt{a}(z_1<z_2) \\ z_3'=z_3-\sqrt{a}(z_1>z_2) \end{cases} \tag{4}$$

If $c=(x_3'-x_2)^2+(y_3'-y_2)^2$, then

$$b=\frac{v_2\sqrt{(x_1-x_2)^2+(y_1-y_2)^2}}{v_1\sqrt{(x_1-x_2)^2+(y_1-y_2)^2+(z_1-z_2)^2}} \tag{5}$$

We can then solve for P_3'. If the vertical error satisfies $\varepsilon=(z_3'-z_3)<0$, or if $b>1$, then

$$\begin{cases} x_2'=(x_1+x_2)/2 \\ y_2'=y_2+k_{xy}\times(x_2'-x_2) \\ z_3'=z_3 \end{cases} \tag{6}$$

On the other hand, if $\varepsilon=(z_3'-z_3)>0$, then

$$\begin{cases} x_2'=(x_3+x_2)/2 \\ y_2'=y_2+k_{xy}\times(x_3'-x_3) \\ z_3'=z_3 \end{cases} \tag{7}$$

where $k_{xy}=(y_2-y_1)/(x_2-x_1)$ is the slope of the projection of the line segment onto the plane $Z=z_2$. P_2' is then obtained by Eqs. (6) and (7), and P_2 is replaced by P_2'. The steps above are repeated until ε is sufficiently small, which yields an estimate of P_3'.

2.2 Step-by-step iterative ray-tracing method

In this paper, source–receiver paths in a layered medium are modified using a step-by-step iterative method. The specific steps (also shown in Fig. 2) are as follows.

(1) The starting point P_0 and endpoint P_n are connected with a straight line. The intersections of the line with each layer (denoted P_1, P_2, P_3, … P_{n-1}) are calculated.

(2) Y_1 is taken as the first interface. A new intermediate refraction point P_1' is calculated between P_0 and P_2 using the dichotomy method, and P_1 is replaced by P_1'. P_1, P_2, P_3, …, P_{n-1} can be obtained in the same way.

(3) Repeat step (2) until $t-t'<\varepsilon$, where t is the travel time of the previous iteration and t' is the current travel time. A series of intermediate points is obtained. The line that connects these points with the two endpoints is taken as the minimum travel time path.

3 Principle of velocity model perturbance

3.1 Very fast simulated annealing with DDrms

In field data, and particularly for surface observations, the location error of a perforation shot is always very large

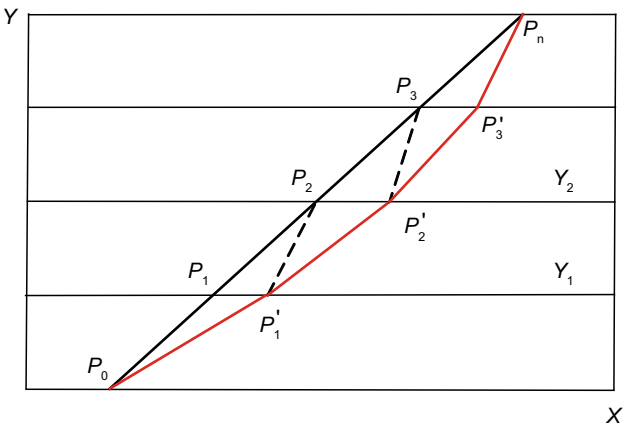

Fig. 2 Iterative node point adjustment (*red solid line* represents the ray path after processing)

when one adopts a velocity model based on a priori well log data. Moreover, part of the data might be missing, which naturally affects the accuracy of the initial model. Therefore, methods of searching for a local optimal velocity model are not applicable. Simulated annealing (SA) is a search algorithm that seeks the global minimum of an objective function in a given model space. There is no need to solve large matrix equations, and constraints can be added easily.

Compared with other techniques, such as the Gaussian–Newton and Levenberg–Marquard methods, SA does not depend on the initial value. As long as the initial annealing temperature is sufficiently high, the method converges stably to the neighborhood of the global minimum. Ingber (1989) presented a very fast simulated annealing (VFSA) algorithm based on iterative calculation of an exponent. Computation was much faster than either the conventional SA algorithm or the standard genetic algorithm (Ingber and Rosen 1992). VFSA has already been used for velocity model estimation based on borehole observations (Pei et al. 2009) by constructing a solution space with six (sets of) parameters:

1. Velocity vector, $\mathbf{V} = (\mathbf{V}_{p1}, \mathbf{V}_{p2}, \mathbf{V}_{p3}, \ldots, \mathbf{V}_{pn})^{T}$, where $\mathbf{V}_{pi}$ denotes the P-wave velocity of layer i.
2. Objective function, $E(\mathbf{V})$. Because perforation shot origin times are inaccurate, we use the RMS error of the time double-difference (DDrms) value, which can be computed from first arrival time differences. The procedure to compute the DDrms value is described below.
3. Initial temperature T_0. The initial temperature must satisfy the requirement that all proposed models are acceptable solutions for the next iteration of the calculation. We choose a small positive number at first, then multiply by a constant value $b > 1$, until the probability of acceptance of each proposed model converges to unity.
4. Temperature annealing parameter, T_k, which for VFSA obeys the relationship

$$T_k = T_0 \exp(-ck^{1/2N}) \tag{8}$$

where T_0 is temperature, c is a constant (for this application, $c = 0.5$ is a suitable value), and N is the total number of layers.
5. A random perturbation to the velocity vector, described below.
6. Termination criteria. In this application, we terminate the algorithm the first time one of the following three conditions is satisfied:
   (a) Temperature T_k is reduced to a certain value or close to zero.
   (b) DDrms value decreases below a predetermined threshold.
   (c) DDrms value does not decrease after multiple iterations.

3.1.1 The objective function

We use the following procedure to construct an objective function based on DDrms values:

1. Select the reference trace with the highest signal-to-noise ratio. This is denoted by the subscript M.
2. Compute the differences between the observed first arrival times of all traces and those of trace M:

$$\Delta t^{\text{obs}} = [t_1 - t_k, t_2 - t_k, \ldots, t_M - t_k].$$

3. Generate an initial velocity model, $\mathbf{V}' = \left[\mathbf{V}'_{p1}, \mathbf{V}'_{p2}, \mathbf{V}'_{p3}, \ldots, \mathbf{V}'_{pn}\right]$, from sonic log data.
4. Calculate theoretical time differences for the reference trace, $\Delta t^{\text{cal}} = [t_1 - t_k, t_2 - t_k, \ldots, t_M - t_k]$, based on $\mathbf{V}'$.
5. Determine the RMS error of the DDrms value using the equations

$$\delta\Delta t = [\Delta t_1^{\text{obs}} - \Delta t_1^{\text{cal}}, \Delta t_2^{\text{obs}} - \Delta t_2^{\text{cal}}, \ldots, \Delta t_n^{\text{obs}} - \Delta t_n^{\text{cal}}] \tag{9}$$

$$E(\mathbf{V}) = \sqrt{\frac{1}{n}\sum\nolimits_{i=1}^{n} \delta\Delta t_i^2} \tag{10}$$

3.1.2 Velocity perturbation vector

The velocity vector is perturbed using the equation

$$\mathbf{V}_i^{k+1} = \mathbf{V}_i^k + x \times S_{\text{fact}} \times \left(\mathbf{V}_i^{\max} - \mathbf{V}_i^{\min}\right) \tag{11}$$

where $\mathbf{V}_i^{\max}$ and $\mathbf{V}_i^{\min}$ are the minimum and maximum values of velocity in layer i, respectively, subject to the constraint $\mathbf{V}_i \in [\mathbf{V}_i^{\min}, \mathbf{V}_i^{\max}]$; S_{fact} is a step-size factor that guarantees the DDrms value decreases stably; and $x \in [-1,1]$ is a random number generated from the equation

$$x = \text{sgn}(\mu - 0.5) T_k \left[\left(1 + \frac{1}{T_k}\right)^{|2\mu - 1|} - 1\right] \tag{12}$$

where sgn denotes the signum function. A suitable value for S_{fact} is approximately 0.1.

3.2 Selecting the optimal velocity model

Before selecting the optimal velocity model, a set of DDrms values and the corresponding velocity models must be obtained. In the simulated annealing process, each time we update the DDrms value, both the DDrms value and the corresponding velocity vector $\mathbf{V}$ are preserved. In the

simulated annealing algorithm, $\mathbf{V}'$ replaces $\mathbf{V}$ if the condition $E(\mathbf{V}') < E(\mathbf{V})$ is satisfied. On the other hand, if $E(\mathbf{V}') > E(\mathbf{V})$, then $\mathbf{V}$ is updated using the replacement probability.

$$P(\mathbf{V} \rightarrow \mathbf{V}') = \exp\left[\alpha \frac{E(\mathbf{V}) - E(\mathbf{V}')}{T}\right] \tag{13}$$

where α is an adjustment parameter. The number of velocity models in the model set is determined by α; the more velocity models are preserved, the greater the likelihood of obtaining reliable results. However, computation time will increase accordingly.

The purpose of establishing a velocity model in this way is to obtain accurate travel times for perforation shots and microseismic events. We mainly focus on the relationships between DDrms value, absolute travel time RMS (i.e., the differences between travel times calculated with the theoretical and synthetic models), and the velocity model RMS for each layer (i.e., the difference between the theoretical and synthetic layer velocities) (Fig. 3).

4 Synthetic examples

In this section, the effects of a hydraulic fracture treatment are simulated to investigate the accuracy of the proposed method. We define a synthetic velocity model with five layers, and exact velocities are given in Table 1. The geophone array geometries and relative perforation shot location are shown in Fig. 4. The exact shot position is $X_{s1} = 830$ m, $Y_{s1} = 840$ m, $Z_{s1} = -1180$ m. This study uses a star-shaped array (6 lines, 96 geophones), as the aim is to place as many geophones as possible in a small area. The initial velocity values for each layer are 950, 1300, 1800, 2800, and 3300 m/s. The simulation requires 2133 s on a notebook computer with a 2.26-GHz Intel® processor. Observed values of first arrival time differences are determined from the true synthetic model using the ray tracing method described above (Fig. 5).

When the minimum DDrms value is determined (here, 2.97e−5 s), the iterative calculation stops and a threshold of 3.97e−5 is set. Ten DDrms values are chosen randomly between the minimum DDrms value and the threshold. The velocity models corresponding to these DDrms values are used to relocate the perforation shot, as shown in Fig. 6. The optimal velocity model is then picked. From the above results, we can see that although there are significant differences between the initial and synthetic velocity models, the perforation shot can be still relocated to its true position; the relocation error is only 1.67 m.

4.1 Sensitivity to the constraints

Here, we consider two main constraints on the viability of adopting a model for use with surface observations. One is the range of *P*-wave velocities used in the model. Increasing this range will increase the solution space; if we use a simulated annealing algorithm with a larger velocity range and parameters that are otherwise unchanged, then source location accuracy and computational efficiency will both be reduced. If the range of velocity variations is too small, then we probably will not obtain a viable result, as shown in Fig. 7. It is therefore desirable to choose a reasonable range of velocity variations in each layer. Generally, the range of velocities in the objective layers is mainly determined from well logging data and local geology.

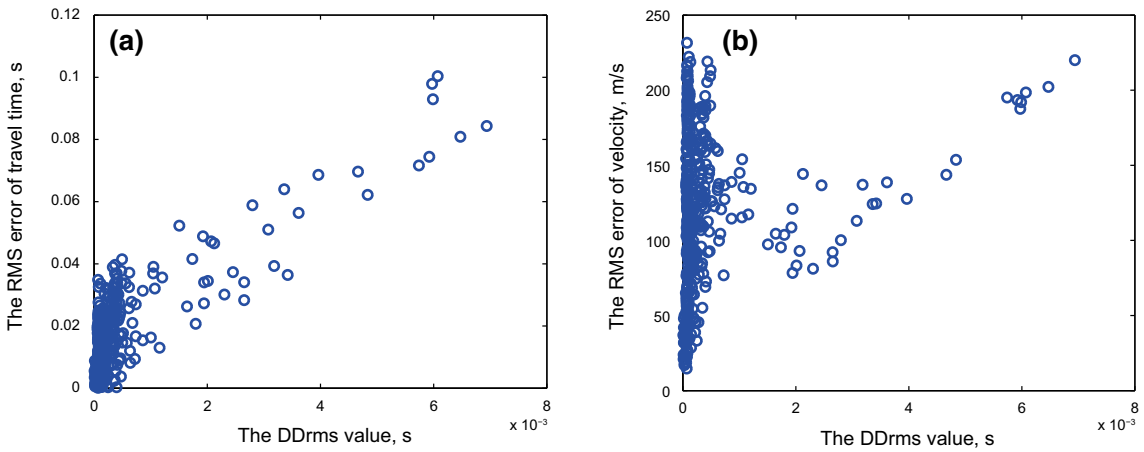

Fig. 3 Sample velocity model distribution. Each *blue circle* represents a velocity model corresponding to one DDrms value. **a** Plot of the relationship between DDrms value and travel time RMS error. The travel time error describes the deviation between the travel time of the perforation shot calculated from the actual medium and that calculated from the velocity model corresponding to the plotted DDrms value. **b** Relationship between DDrms value and velocity model RMS. The model error reflects differences between the velocity model and the actual medium

Table 1 Synthetic velocity model parameters

Layer	Depth, m	Synthetic velocity model, m/s	Velocity constraint range ($\mathbf{V}_{min} - \mathbf{V}_{max}$), m/s
1	0–200	1200	600–1300
2	200–500	1600	1000–1800
3	500–700	2200	1600–2400
4	700–900	3200	2400–3600
5	900–1200	3800	3000–4200

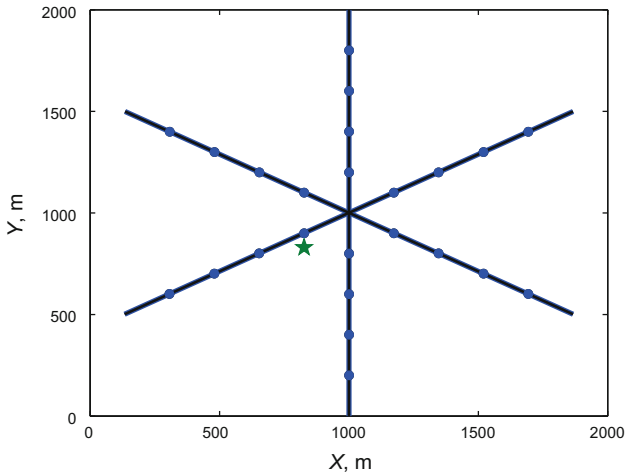

Fig. 4 Geometry of recording stations and perforation shot. Each station has 4 geophones, for a total of 96 sensors. *Black lines* represent the arms of the star-patterned array. *Blue dots* represent geophone positions. The *green star* represents the position of the perforation shot

Another constraint is the number of surface geophones, which determines the number of time double-differences available for the inversion. The same termination conditions are used for the SA algorithm, and adding surface geophones improves the convergence of the DDrms value, as shown in Fig. 8. However, the algorithm requires more computation time to converge. Less accurate travel time information is obtained when DDrms is reduced to a small value, and it can be the case that no acceptable velocity model is obtained at all. Figure 8 compares the velocity calibration results with different numbers of surface geophones; the termination conditions are the same for all simulations. Using the same line pattern as in Fig. 4, the number of geophones increases or decreases uniformly in each line.

The minimum DDrms value of Fig. 8a is 1.3e−6. The minimum DDrms value in Fig. 8b–d is less than 2.5e−6 s. As shown in Fig. 8, reliable location results are more likely when a large number of surface geophones are used.

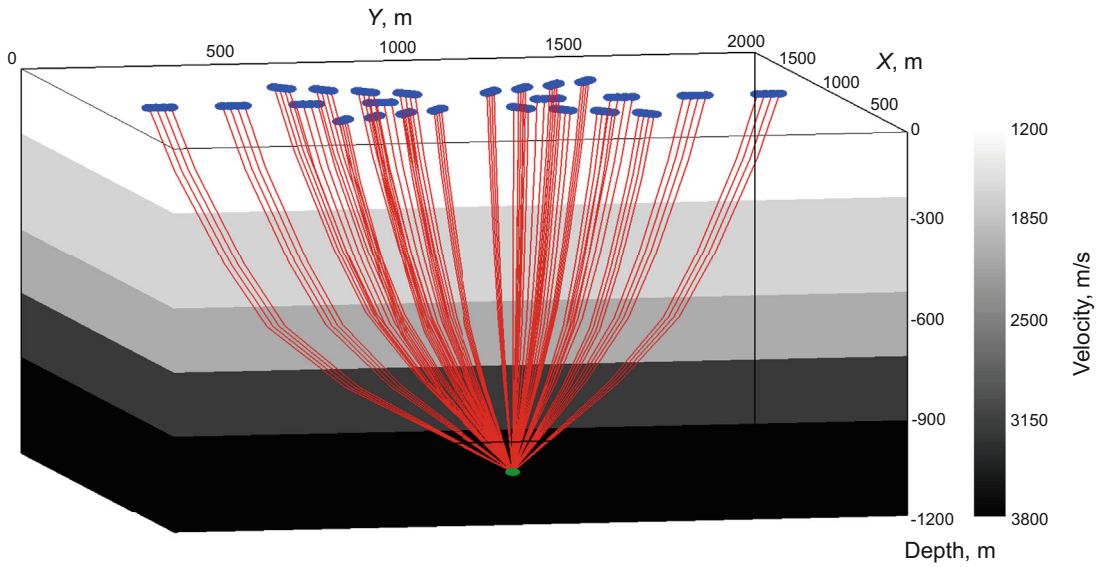

Fig. 5 Velocity model and ray paths. The *green dot* represents the perforation position, *red lines* represent ray paths, and *blue dots* represent receivers

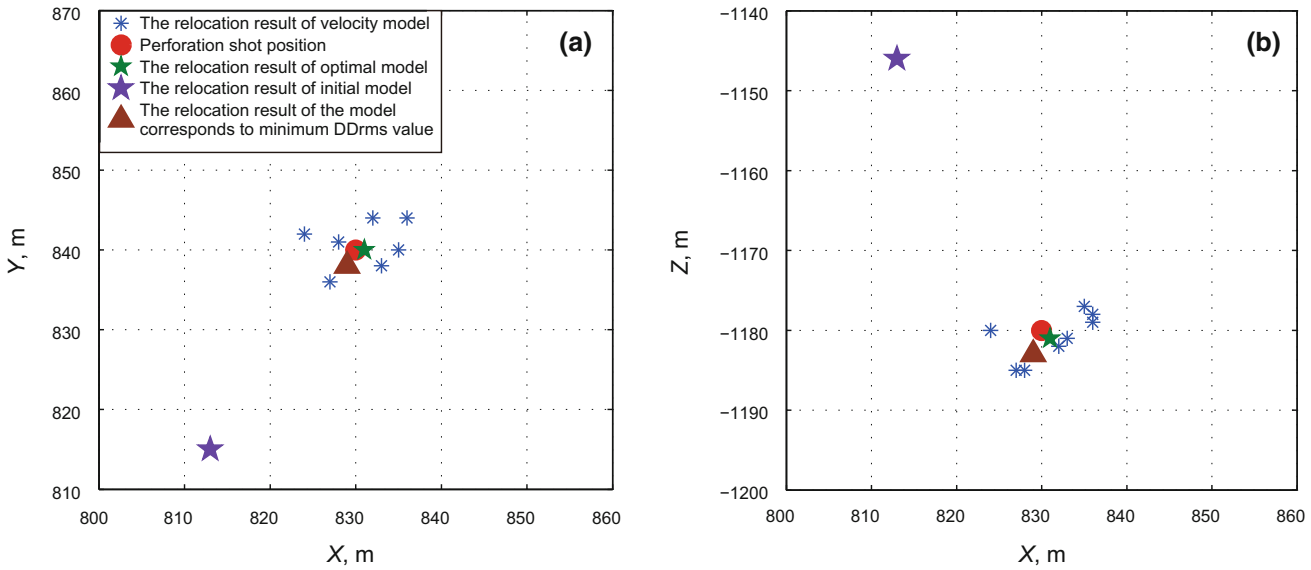

Fig. 6 Calculated perforation shot locations using 10 sample velocity models. The selected models corresponded to DDrms values within a certain range of the minimum DDrms value. **a** The *top* view, **b** the *side* view

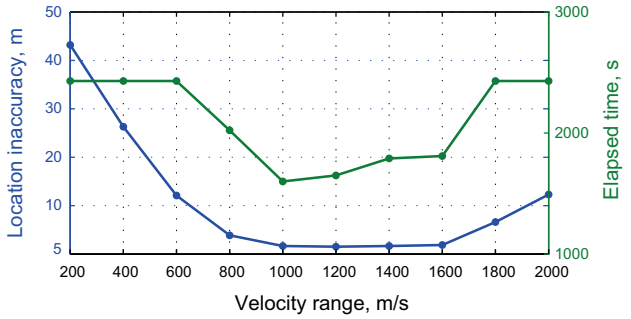

Fig. 7 Influence of velocity range on the accuracy and efficiency of the source location. The *horizontal axis* represents the total range of *P*-wave velocities in the synthetic velocity structures of different tests

However, increasing the number of surface arrays arbitrarily may lead the reduction of DDrms value to be difficult. In this case, more computation time is needed; notably, increasing the number of rays also increases the forward calculation time.

4.2 The sensitivity to picking errors

Calibrating a velocity model for microseismic event location requires accurate information about perforation shots. In actual situations, seismic signals recorded by geophones are usually contaminated by noise, which may cause picking errors (Rodriguez et al. 2012; Song et al. 2010; Tan et al. 2014). Compared with borehole observations, the picking errors of *P*-wave arrivals are relatively large at the surface. This will affect the proposed technique. Therefore, to model our algorithm's sensitivity to picking errors, we add a set of random picking errors to the synthetic arrival times at each receiver, ranging from 0 to 5 % of the calculated travel time. We use the same stop condition as in the numerical experiments above. The algorithm terminates when DDrms value reaches 7.84e−4 s. A threshold of 8.84e−4 s is set; 10 velocity models are selected to relocate the perforation shot, and an optimal velocity model is picked out by the method described above.

Figure 9 shows that the perforation shot can still be located close to its true position, despite picking errors. The location inaccuracy is again within 2 m, and relatively accurate results can still be obtained. The velocity model can be considered an "equivalent" velocity model. Because of the large discrepancies between the recovered velocity model and the true model, large errors are possible when locating microseismic events far from the perforation.

In Fig. 10, the velocity models used in Fig. 9 are used to locate a synthetic microseismic event (true hypocenter 534, 532, −1165). This illustrates the relative accuracy of microseismic event location using these velocity models. Figure 11 illustrates the relationship between first arrival time picking errors and minimum DDrms values, using the same stop conditions as for the previous tests.

Figure 10 confirms that for microseismic events located far from the perforation, the optimal velocity model for the perforation shot introduces an inherent location error. Figure 11 suggests that increasing picking errors will increase location errors; for example, if picking errors reach 20 % of computed travel times, locations of microseismic events will be poorly constrained. The main reason

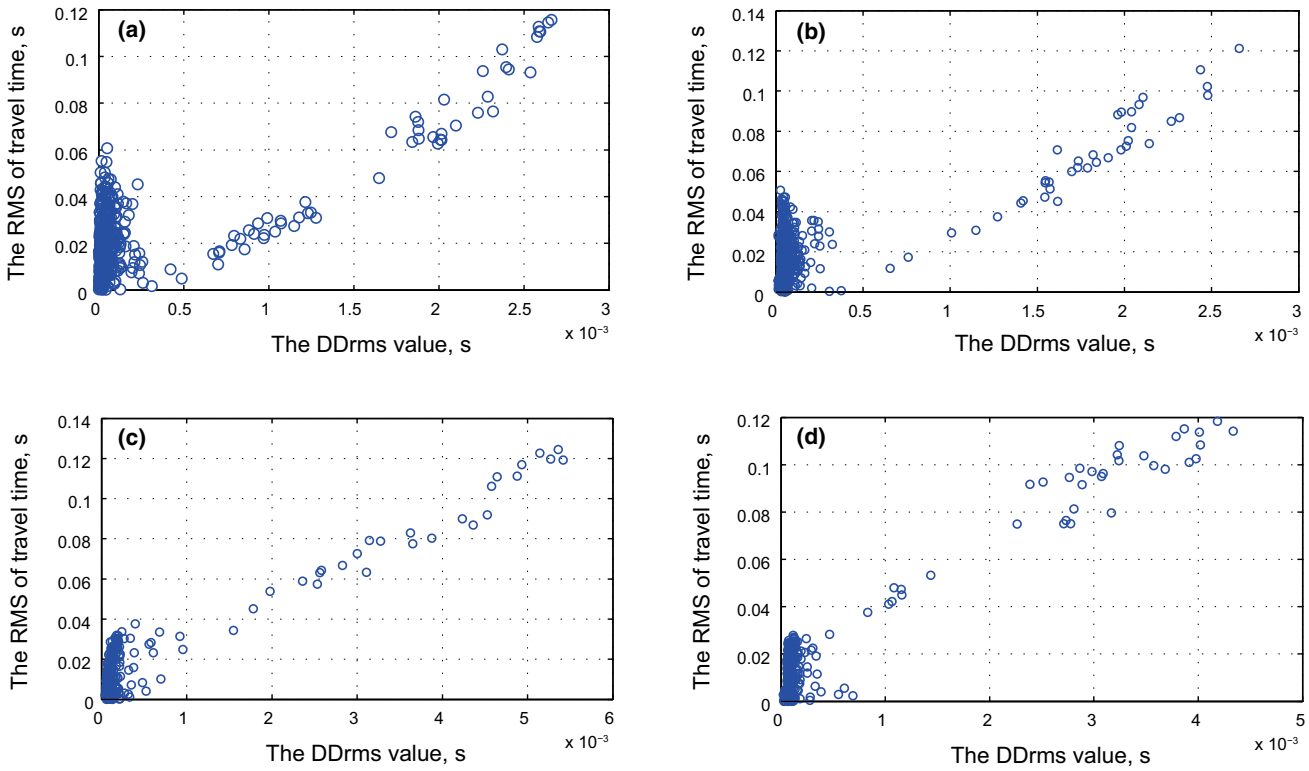

Fig. 8 Comparative plots of tomography inversion results with different constraints. The inversion takes approximately 47 s with 6 geophones in (**a**); 232 s with 24 geophones in (**b**); 813 s with 48 geophones in (**c**); and 3137 s with 96 geophones in (**d**). Legends are the same as for Fig. 3

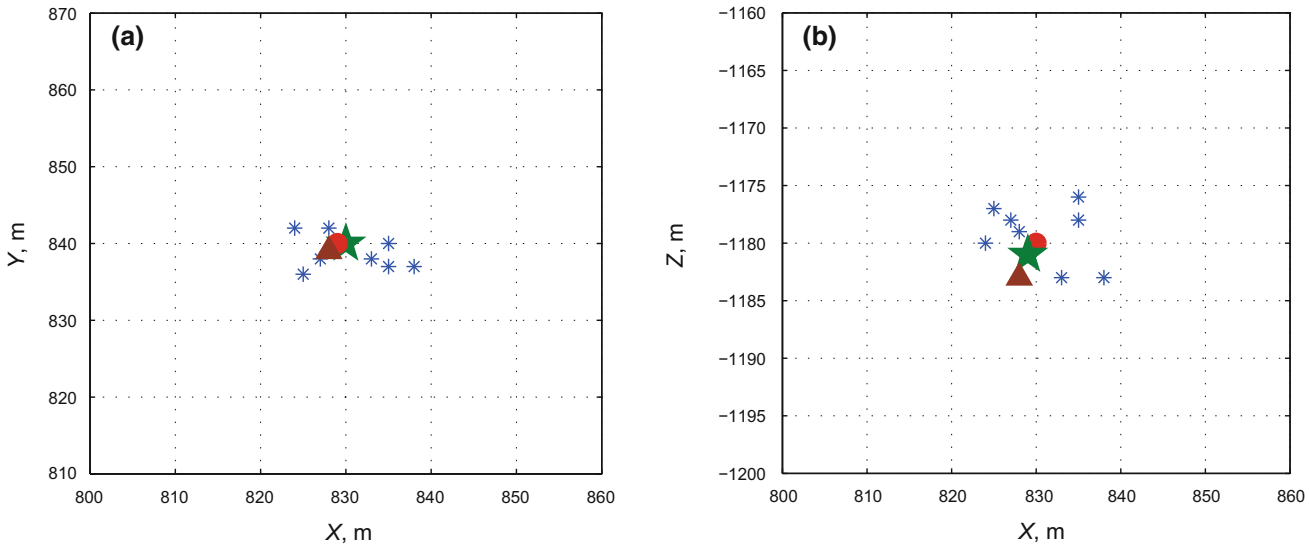

Fig. 9 Relocation of a perforation shot using data with picking errors, legends are the same as for Fig. 6. **a** *Top* view, **b** *Side* view

for this is that the process of reducing the DDrms value is influenced by the picking errors; when picking errors are large, the DDrms value cannot be reduced to a sufficiently small value, and this reduces the chances to obtain a meaningful velocity model.

5 Field data experiments

In this section, we test our algorithm's performance on data recorded by an experiment in Shanxi province, China. As shown in Fig. 12, six survey lines were deployed in this

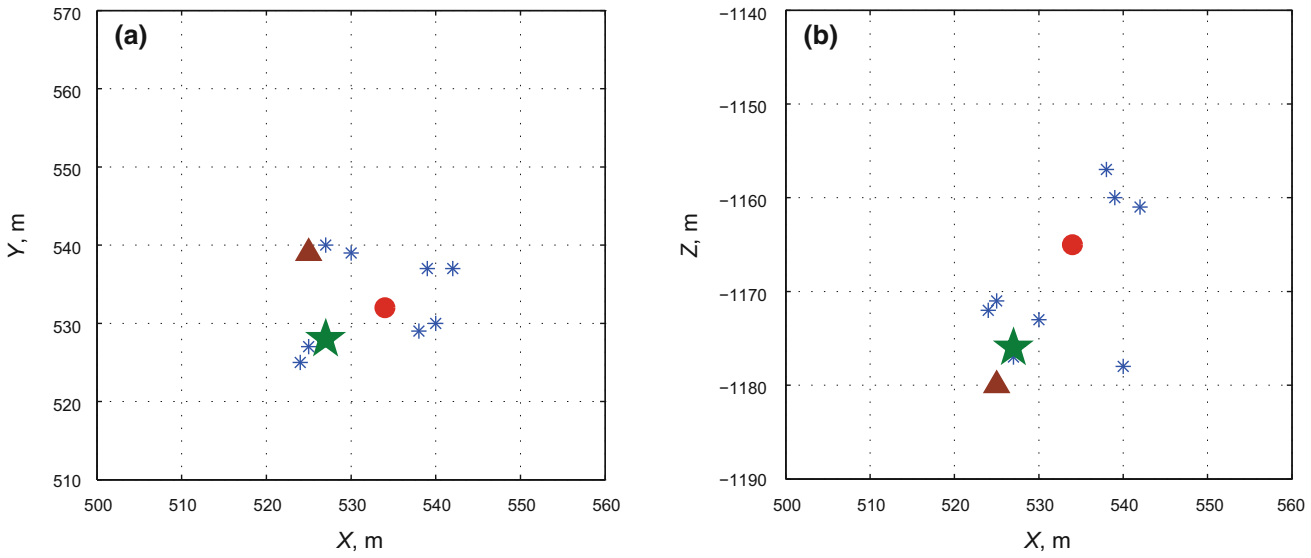

Fig. 10 The location result of microseismic event using the data with picking errors, legends are the same as for Fig. 6. **a** *Top* view, **b** side view

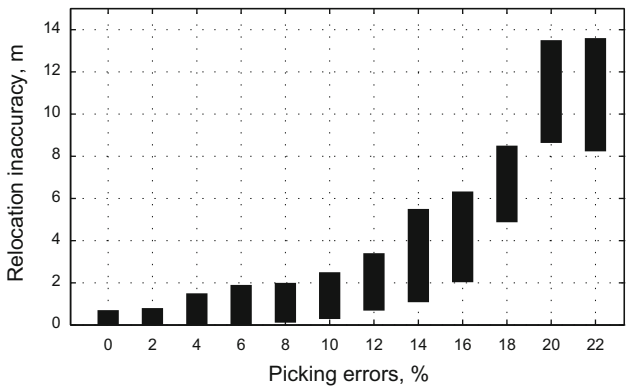

Fig. 11 Relationship between picking errors of first arrival times and relocation inaccuracy. The *x*-axis represents the maximum values of picking errors added to the synthetic data; the *thick black lines* indicates the range of relocation inaccuracies after 100 trials

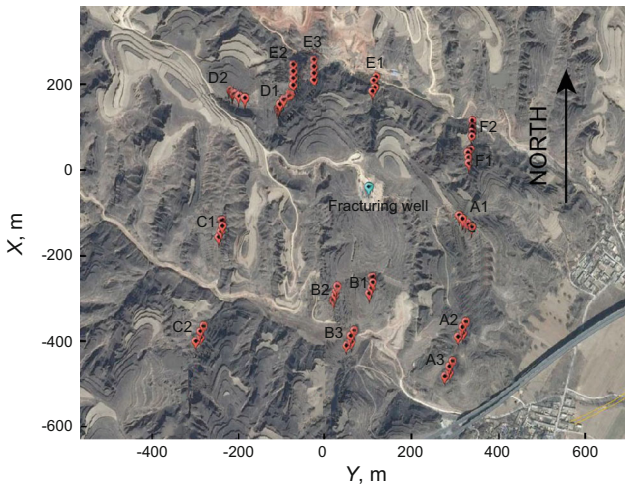

Fig. 12 Microseismic monitoring array geometry. Geophones are arranged in a *star-like* surface array around production wells

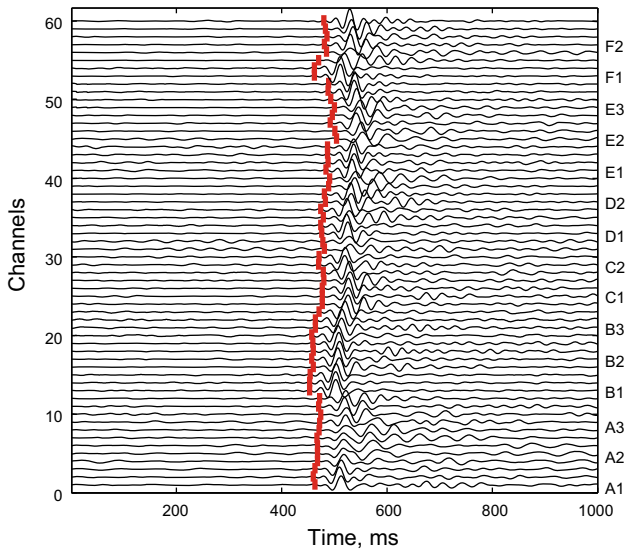

Fig. 13 Perforation shot monitoring records for the surface geophones in Fig. 12. The *x*-axis represents time since the beginning of the record. The *y*-axis corresponds to geophone channel numbers

experiment, with two or three data loggers per line. Each data logger was equipped with four vertical-component geophones, with a horizontal sensor spacing of 20 m along the line. The first geophone of each survey line was placed at a fixed distance from the center of the array, to ensure that the data loggers were evenly distributed and all sensors were far enough from the injection well to minimize noise from processes related to injection (e.g., mechanical pump noise). The position of the straight well is at the center of the observation system; the wellhead coordinates were (−68.025, 107.258, −1.34) under the unified GPS

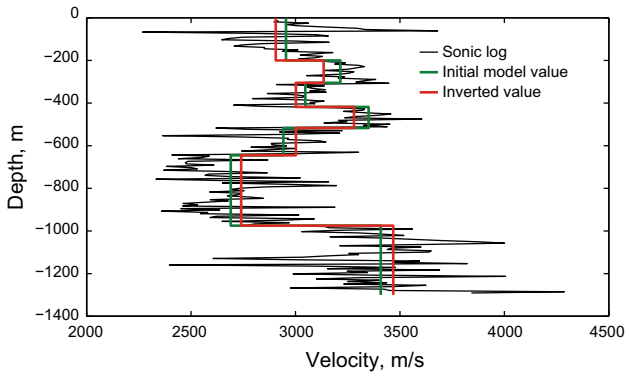

Fig. 14 Inversion results, showing initial and optimal velocity models

observation system we defined. The perforation (fracturing point) coordinates are (107.258, −68.025, −1197.8). The maximum geophone elevation is −3.87 m and the minimum is −102.73 m. Because the waveforms of Fig. 13 are not in good agreement, we obtain first arrival picks for each geophone manually. Figure 14 shows the initial velocity obtained from well logging data, and the optimal velocity model obtained by the method of this paper. The velocity structure was divided into seven layers, based on sonic logs (Table 2). Layer boundaries corresponded to sudden velocity changes. The number of layers and their respective thicknesses do not need to be a constraint. The perforation positions obtained from the initial velocity model contain significant errors, as shown in Fig. 15. However, the perforation could be located close to its true position using models obtained by inversion. Therefore, we infer that the final velocity model is suitable for microseismic event locations. The VFSA algorithm reduced the DDrms value from 0.0215 s to 4.4e−4 s. To improve the accuracy of the inversion, we set a selection threshold of 6.4e−4 s for candidate velocity models. Fifty models with DDrms values between the threshold and the minimum were selected. These were used to relocate the perforation shot, and an optimal velocity model was picked based on the results. From Fig. 15, compared with the initial velocity model, the perforation shot can be located very close to its actual position; the location inaccuracy is 5.23 m. Therefore, we conclude that the velocity model obtained by our method is suitable for microseismic event location.

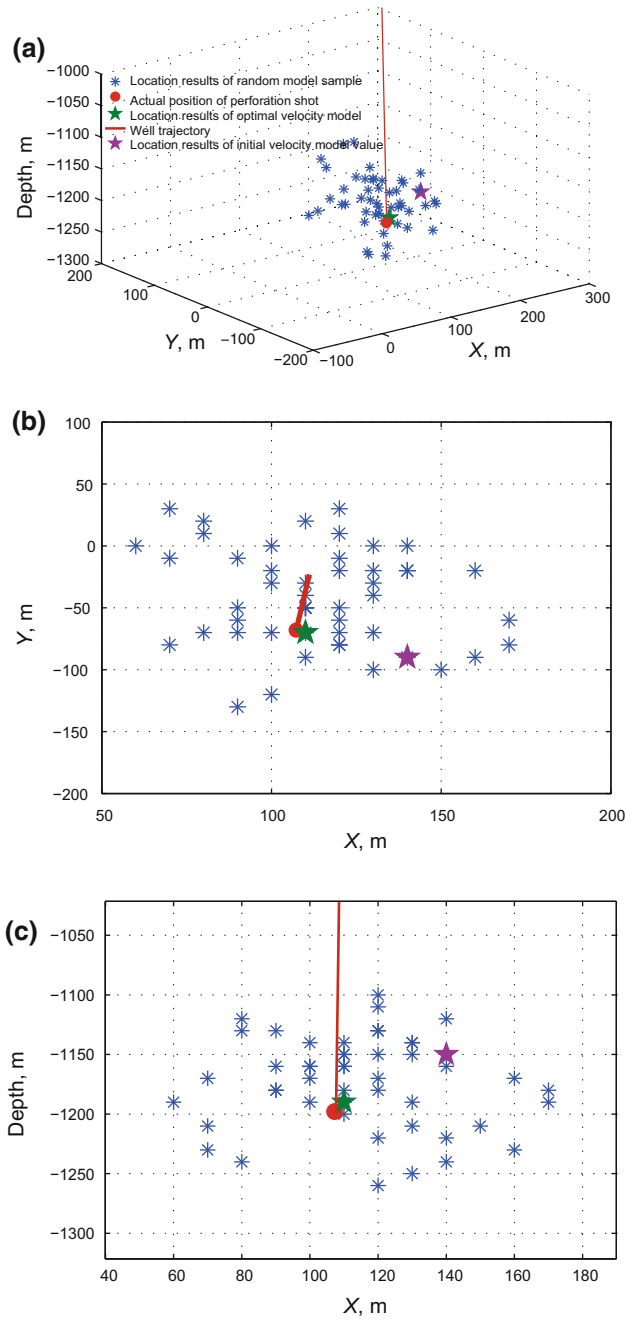

Fig. 15 Location results based on 50 candidate velocity models. Models are selected if their final DDrms value lies within the range of the minimum DDrms value; each model is used to locate the perforation shot independently. **a** Three-dimensional figure. **b** *Top* view. **c** *Side* view

6 Conclusion

In this paper, we present a non-linear inversion method for the calculation of velocity models suitable for locating microseismic events with surface sensor data. The proposed technique is based on the RMS error of time double-differences, which are determined from surface records of perforation shots. The DDrms value is minimized using a VFSA algorithm, and velocity model viability is evaluated based on the accuracy of perforation shot relocations. This technique can overcome many of the difficulties caused by monitoring hydraulic fractures with surface instruments alone. Using tests on synthetic and field data, our interpretations and conclusions are as follows.

Table 2 Stratum velocity structure parameters

Layer	Depth, m	Starting velocity model, m/s	Velocity constraint range ($\mathbf{V}_{min} - \mathbf{V}_{max}$), m/s
1	0–200	2954.5	2650–3200
2	200–305	3214.5	3100–3500
3	305–418	3047.8	2800–3200
4	418–517	3348.6	3200–3500
5	517–645	2942.2	2600–3300
6	645–975	2690.1	2400–3000
7	975–1300	3408.2	3000–3800

1. The proposed technique does not strongly depend on the initial velocity model, and can also overcome the problem of inaccurate perforation shot origin times. However, due to complex local geology and a lack of available information, the velocity model inversion is non-unique. Therefore, whether or not a velocity model is suitable for microseismic event location is determined based on the accuracy of perforation-shot relocation.
2. Constraints on velocity structure have an effect on the proposed technique's results. Reasonable velocity constraints should be imposed on each layer; if these are improperly selected, analyst errors will negatively affect the outcome. Second, the DDrms value should be reduced as much as possible; the smaller the DDrms value, the more reliable the optimal velocity model. When using the same simulated annealing termination condition as our examples, more surface geophones are needed.
3. If the arrival times of a perforation shot include significant picking errors, it may be the case that DDrms values do not converge to a reasonable minimum. This can greatly influence the effectiveness of our technique, so it is imperative to minimize picking errors.
4. When processing real field data, after velocity model calibration, a perforation shot could be located to its actual position. Thus, we believe nearby microseismic events can be located with confidence. However, due to many limitations of microseismic monitoring operations, we do not expect to obtain an accurate velocity model from only one perforation shot; this implies a certain risk for microseismic events located far from the perforation. Therefore, it may be necessary to introduce more complex velocity models and source information in our application.

Acknowledgments This study is supported by the National Natural Science Foundation of China (No. 41074074).

References

Anikiev D, Valenta J, Staněk F, et al. Joint location and source mechanism inversion of micro-seismic events: benchmarking on seismicity induced by hydraulic fracturing. Geophys J Int. 2014;198(1):249–58.

Bardainne T, Gaucher E. Constrained tomography of realistic velocity models in microseismic monitoring using calibration shots. Geophys Prospect. 2010;58(5):739–53.

Concha D, Fehler M, Zhang HJ, et al. Imaging of the Soultz enhanced geothermal reservoir using microseismic data. In: 35th Workshop on Geothermal Reservoir Engineering Stanford University. 2010; SGP-TR-188.

Gao EG, Xu GM. A new kind of step by step iterative ray tracing method. Chin J Geophys. 1996;39(Supplement):302–8 **(in Chinese)**.

Grechka V, Singh P, Das I. Estimation of effective anisotropy simultaneously with locations of microseismic events. Geophysics. 2011;76(6):WC143–55.

Ingber L, Rosen B. Genetic algorithms and very fast simulated reannealing: a comparison. Math Comput Model. 1992;16(11):87–100.

Ingber L. Very fast simulated re-annealing. Math Comput Model. 1989;12(8):967–73.

Li F, Xu T, Wu ZB. Segmentally interactive ray tracing in 3-D heterogeneous geological models. Chin J Geophys. 2013;56(10):3514–22 **(in Chinese)**.

Liang BY, Chen S, Leng CB, et al. Development of microseismic monitoring for hydro-fracturing. Progr Geophys. 2015;30(1):0401–10.

Pei DH, Quirein JA, Cornish BE, et al. A very fast simulated annealing (VFSA) approach for joint-objective optimization. Geophysics. 2009;74(6):WCB47–55.

Pei DH, Quirein JA, Cornish BE, et al. Velocity calibration using microseismic hydraulic fracturing perforation and string shot data. In: 49th Annual Logging Symposium. 2008; SPWLA: 2008-H.

Quirein JA, Grable J, Cornish BE, et al. Microseismic fracture monitoring. In: Annual Logging Symposium. Society of Professional Well Log Analysts. 2006.

Rodriguez IV, Bonar D, Sacchi M. Microseismic data denoising using a 3C group sparsity constrained time-frequency transform. Geophysics. 2012;77(2):21–9.

Song FX, Kuleli SH, Toksöz NM. An improved method for hydrofracture-induced microseismic event detection and phase picking. Geophysics. 2010;75(6):A47–52.

Tan YY, He C, Hou XC, et al. Detection and location of microseismic events with low signal-to-noise ratios. In: International Petroleum Technology Conference. 2014; Kuala Lumpur, Malaysia.

Tan YY, He C, Zhang HL. Time difference-based velocity model inversion for microseismic event location. In: SEG Houston 2013 Annual Meeting. 2013; Segam: 2013-0165.

Usher PJ, Angus DA, Verdon JP. Influence of velocity model and source frequency on microseismic waveforms: some implications for microseismic locations. Geophys Prospect. 2013;61(Suppl. 1):334–45.

Waldhauser F, Ellsworth WL. A double-difference earthquake location algorithm: method and application to the Northern Hayward Fault, California. Bull Seismol Soc Am. 2000;90(6):1353–68.

Wang CL, Cheng JB, Yin C, et al. Microseismic events location of surface and borehole observation with reverse-time focusing using interferometry technique. Chin J Geophys. 2013;56(9):3184–96 **(in Chinese)**.

Wang H, Chang X. 3 D ray tracing method based on graphic structure. Chinese Journal of Geophysics. 2002;43(4):534–41 **(in Chinese)**.

Warpinski NR, Sullivan RB, Uhl JE, et al. Improved microseismic fracture mapping using perforation timing measurements for velocity calibration. SPE J. 2005;10:14–23.

Xu T, Xu GM, Gao EG. Block modeling and shooting ray tracing in complex 3-D media. Chin J Geophys. 2004;47(6):1118–26 **(in Chinese)**.

Zhang D, Fu XR, Yang Y, et al. 3-D Seismic ray tracing algorithm based on LTI and partition of grid interface. Chin J Geophys. 2009a;52(9):2370–6.

Zhang HJ, Sarkar S, Toksöz MN, et al. Passive seismic tomography using induced seismicity at a petroleum field in Oman. Geophysics. 2009b;74(6):WCB57–69.

Zhang HJ, Thurber CH. Double-difference tomography: the method and its application to the Hayward Fault, California. Bull Seismol Soc Am. 2003;93(5):1875–89.

Zhang MG, Cheng BJ, Li XF. A fast algorithm of shortest path ray tracing. Chin J Geophys. 2006a;18(1):146–50 **(in Chinese)**.

Zhang MG, Jia YG, Wang MY, et al. A global minimum travel time ray tracing algorithm of wave front expanding with interface points as secondary sources. Chin J Geophys. 2006b;49(4):1169–75 **(in Chinese)**.

Zhang XL, Zhang F, Li XY. The influence of hydraulic fracturing on velocity and microseismic location. Chin J Geophys. 2013a;56(10):3552–60 **(in Chinese)**.

Zhang XL, Zhang F, Li XY, et al. The influence of hydraulic fracturing on velocity and microseismic location. Chin J Geophys. 2013b;56(10):3552–60.

Zhao HY, Zhang MG. Tracing seismic shortest path rays in anisotropic medium with rolling surface. Chin J Geophys. 2014;18(1):2910–7 **(in Chinese)**.

Zhou RM, Huang LJ, Rutledge J. Microseismic event location for monitoring CO_2 injection using double-difference tomography. Lead Edge. 2010;29(2):208–14.